Appl. Phys. B (2017) 123:93
DOI 10.1007/s00340-017-6679-x

Applied Physics B
Lasers and Optics

Tunable organic distributed feedback dye laser device excited through Förster mechanism

Naoto Tsutsumi[1] · **Taiki Hinode**[2]

Received: 24 August 2016 / Accepted: 20 February 2017 / Published online: 12 March 2017

Abstract Tunable organic distributed feedback (DFB) dye laser performances are re-investigated and characterized. The slab-type waveguide DFB device consists of air/active layer/glass substrate. Active layer consisted of tris(8-quinolinolato)aluminum (Alq_3), 4-(dicyanomethylene)-2-methyl-6-(4-dimethylaminostyryl)-4H-pyran (DCM) dye, and polystyrene (PS) matrix. Effective energy transfer from Alq_3 to DCM through Förster mechanism enhances the laser emission. Slope efficiency in the range of 4.9 and 10% is observed at pump energy region higher than 0.10–0.15 mJ cm^{-2} (lower threshold), which is due to the amplified spontaneous emission (ASE) and lasing. Typical slope efficiency for lasing in the range of 2.0 and 3.0% is observed at pump energy region higher than 0.25–0.30 mJ cm^{-2} (higher threshold). The tuning wavelength for the laser emission is ranged from 620 to 645 nm depending on the ASE region.

1 Introduction

Organic solid-state lasers (OSSLs) have been developed extensively in the past two decades [1, 2], because of the easy modification of the optical gain matrix, the easy fabrication of devices by spin-coating technique or deposition technique, as well as the use of several resonators, vertical Fabry–Perot microcavity with distributed Bragg reflector (DBR) mirror, microring resonator, microdisc resonator, and planar waveguide with distributed feedback (DFB) or DBR resonator. Photolithography, electron-beam lithography, and the interference of laser beams are commonly used to fabricate the DFB and DBR structures in substrates and active layers. In organic systems, the excitation energy frequently meets the energy quenching due to π–π stacking and dipole–dipole interaction between molecules, and these unfavorable interactions lead to increased overall loss; thus, it increases the lasing thresholds and decreases the efficiencies [2]. Molecular design of the organics for high laser performances is directed towards improving fluorescence properties in laser devices. One solution is the use of a dendrimer with core for emission and highly branched surfaces to limit π–π stacking [3–5]. Among them, one such system is truxene-based star-shaped oligofluorenes, which exhibited ultralow lasing DFB thresholds less than 1 μJ cm^{-2} (under femtosecond laser pumping) [5]. The guest–host system is another type of solution. Pump energy is absorbed by a molecule with higher energy gap, and the excited energy efficiently transfers from excited molecule to emitting molecules through Förster mechanism. The combination of tris(8-quinolinolato)aluminum (Alq_3) with higher energy gap as a host and 4-(dicyanomethylene)-2-methyl-6-(4-dimethylaminostyryl)-4H-pyran (DCM) with lower energy gap as a emitter is archetype of a guest–host system [6–8]. Recently, low threshold of 4 μJ cm^{-2} was reported in photonic crystal nanobeam cavity deposited by Alq_3 and DCM [9]. In our former study [10–12], DFB laser performances of Alq_3/DCM in polymer matrix have been reported. However, the slope efficiency has not been investigated.

In this paper, DFB laser performances are characterized in the waveguide device consisting of Alq_3, DCM dye, and

✉ Naoto Tsutsumi
tsutsumi@kit.ac.jp

[1] Faculty of Materials Science and Engineering, Kyoto Institute of Technology, Matsugasaki, Sakyo, Kyoto 606-8585, Japan

[2] Department of Macromolecular Science and Engineering, Graduate School of Science and Technology, Kyoto Institute of Technology, Matsugasaki, Sakyo, Kyoto 606-8585, Japan

polystyrene (PS). Slope efficiency and lasing threshold for laser emission are investigated in a three-layer waveguide device, air/active layer (Alq_3/DCM/PS)/glass substrate. The contents of Alq_3 and DCM are widely varied: Alq_3 concentration ranged from 20 to 60 wt%, and DCM concentration from 0.5 to 5 wt%. The energy transfer dynamics between the excited Alq_3 and DCM is involved to discuss the slope efficiency and the threshold for lasing. The appropriate concentration of Alq_3 and DCM in PS matrix is discussed.

2 Experimental

PS (Wako, Japan) was purified by a reprecipitation. DCM (Aldrich, USA) and Alq_3 (Tokyo Chem. Ind., Japan) were used as received. A chloroform solution of PS with DCM and Alq_3 was spin-coated on a glass substrate at 1700 or 2000 rpm for 30 s to form the waveguide-type DFB laser device.

Laser emission of the waveguide-type DFB laser device was monitored using a Llyod mirror technique. A frequency-tripled Nd:YAG pulse laser delivering a 30 ps pulse at λ_p = 355 nm with a 10 Hz repetition rate was used as a pumping source. The pumping laser was focused on the waveguide with a cylindrical lens (f = 300 mm) to make a stripe shape of the exciting beam (3.25 mm long by 0.033 mm wide). A Tokyo Instruments multi-channel analyzer used was equipped with 1200 lines/500 nm gratings and an Andor iDus charge-coupled device (CCD). A UV–Vis absorption spectrum was measured using a Shimadzu UV-2101PC spectrophotometer. The photoluminescence (PL) spectrum was recorded using a Shimadzu RF-1500 fluorophotometer.

Lasing energy was monitored using an Ophir photodiode-type pyrometers PD10 and PD10-PJ with a Nova II Display. The index of refraction (n) of the waveguide was determined using a prism coupling method, in which the evanescent wave penetrates into the waveguide film at the specific mode angle at each mode (m = 0, 1, 2, …) (m-line method). The laser sources were a polarized He–Ne laser (632.8 nm) and a laser diode (830 nm). Waveguide and a prism of Hoya TaFD21 with n = 1.926 at 632.8 nm and n = 1.909 at 830 nm were coupled with an air gap. Indices of refraction measured are summarized in Table 1. Index of refraction at lasing peak $n(\lambda)$ was evaluated using a one-oscillator Sellmeier dispersion formula of.

$$n^2(\lambda) - 1 = \frac{q}{1/\lambda_0^2 - 1/\lambda^2} + A, \quad (1)$$

where q is a measure of the oscillator strength, A is a constant containing the sum of all the other oscillators, and the absorption wavelength of dominant oscillator λ_0 of 392 nm. The values of q and A were determined using refractive indices measured at 632 and 830 nm for TE mode and for TM mode, respectively.

Table 1 Summary of indices of refraction measured using m-line method

	632.8 nm		830 nm	
	TE	TM	TE	TM
PS/Alq_3/DCM = 100/0/0	1.586	1.587	1.577	1.575
PS/Alq_3/DCM = 99/0/1	1.593	1.598	1.582	1.587
PS/Alq_3/DCM = 89/10/1	1.608	1.610	1.597	1.601
PS/Alq_3/DCM = 69/30/1	1.616	1.618	1.601	1.603
PS/Alq_3/DCM = 59/40/1	1.642	1.643	1.624	1.626
PS/Alq_3/DCM = 49/50/1	1.659	1.659	1.639	1.641

3 Results and discussion

3.1 Determination of optimized content of Alq_3 and DCM for organic DFB laser

The threshold and the slope efficiency are important factors to evaluate the laser performances in organic DFB lasers. As discussed in previous paper [10], the efficient energy transfer from Alq_3 to DCM assists the laser performances. Thus, the effective energy transfer from Alq_3 to DCM is an important factor for the present laser device. To concentrate the excitation energy to DCM sites effectively, the concentrations of Alq_3 and DCM were optimized.

Figure 1 shows the lasing profile for PS/Alq_3/DCM (69/30/1 by wt). Laser spectrum and peak intensity are plotted as a function of pump energy in Fig. 1a, b, respectively. Narrow laser spike (line width = 0.2 nm) appears in a large amplified spontaneous emission (ASE). Output energy is plotted as a function of pump energy in Fig. 1c. Lasing threshold is determined to be 0.23 mJ cm^{-2} in Fig. 1b. Slope efficiency of 6.1% is measured at lower pump energy region up to 0.6 μJ (0.25 mJ cm^{-2}) and that of 1.8% is at pump energy higher than 0.6 μJ (0.25 mJ cm^{-2}).

Figure 2 shows the same lasing profile for PS/Alq_3/DCM (49/50/1 by wt.). The lasing spike (peak) is detected at the pumping energy of 0.15 mJ cm^{-2}, and the peak intensity increases by increasing the pump energy as shown in Fig. 2a. The peak intensity is plotted as a function of pump energy, and the lasing threshold of 0.15 mJ cm^{-2} is evaluated in Fig. 2b. Output energy is plotted as a function of pump energy in Fig. 2c. Two slope efficiencies for laser emission, the slope between pump energy and output energy, are evaluated at the pump energy region above the threshold. The slope efficiency of 7.3% is measured at pump energy up to 0.52 μJ (0.24 mJ cm^{-2}) and that of 2.8% at pump energy higher than 0.52 μJ (0.24 mJ cm^{-2}).

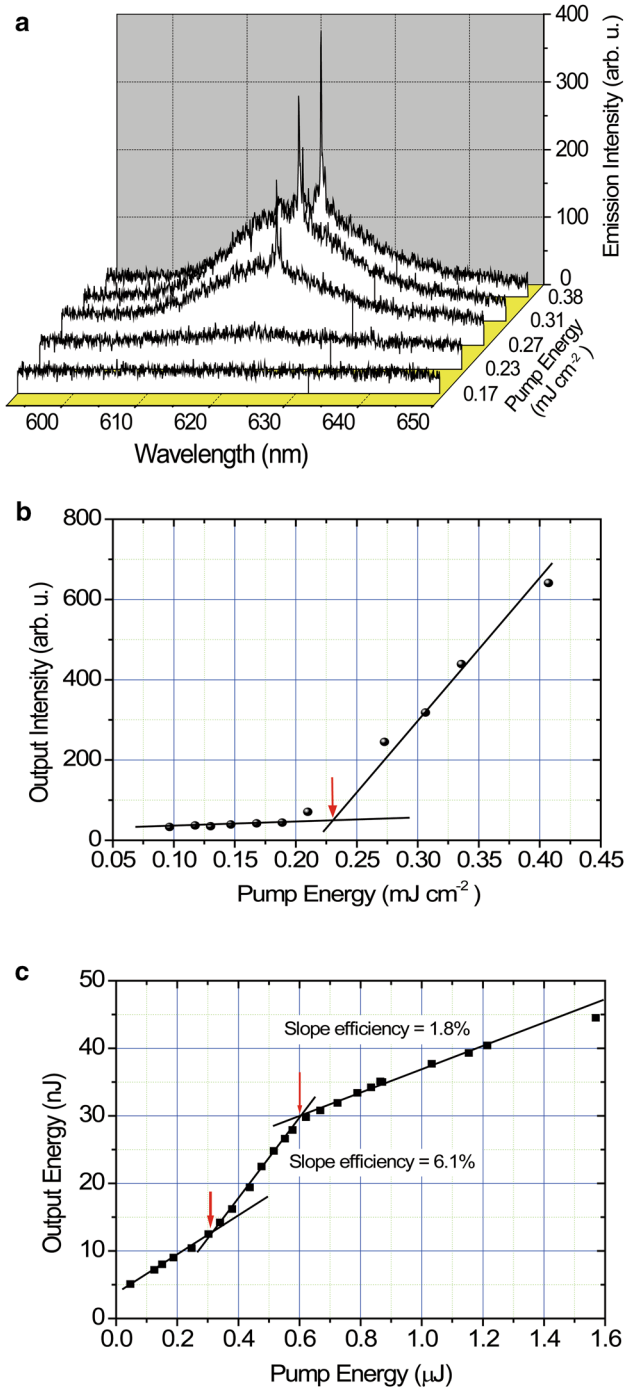

Fig. 1 Lasing performances for PS/Alq_3/DCM (69/30/1 by wt.). **a** Laser emission spectrum with various pump energies. **b** Laser peak intensity as a function of pump energy. Intersection of two lines shows threshold for laser emission. *Red arrow* shows threshold. **c** The plots of pump energy and output energy. Slope efficiency is determined. *Red arrows* show threshold

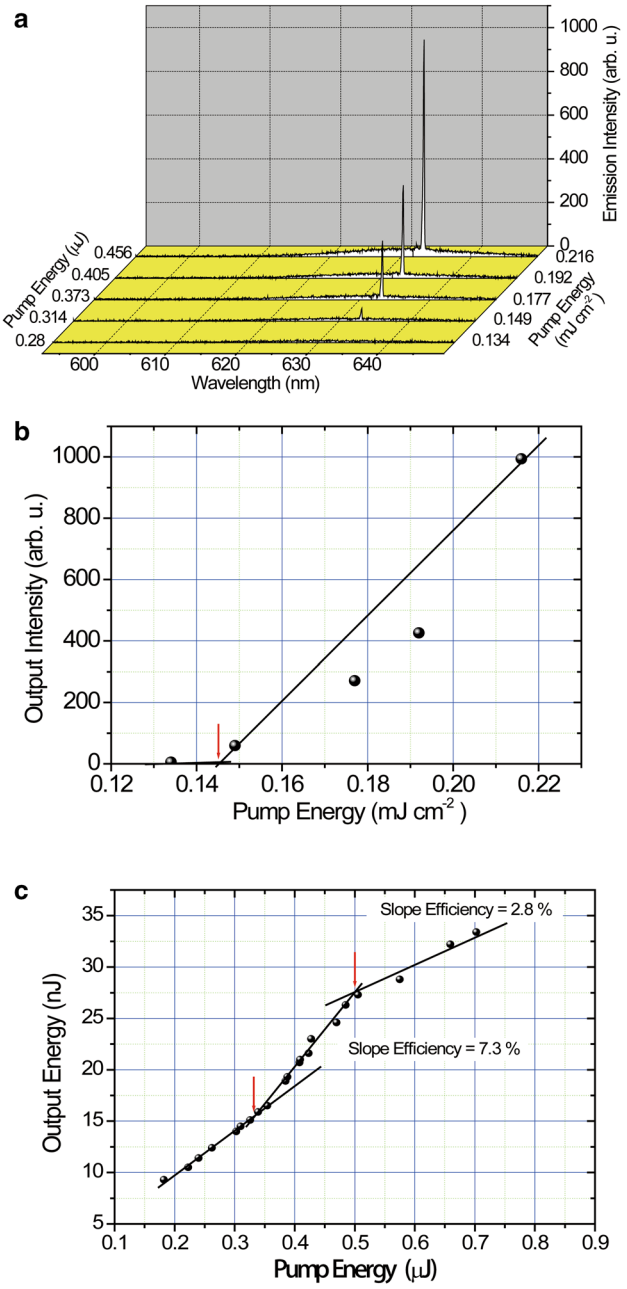

Fig. 2 Lasing performances for PS/Alq_3/DCM (49/50/1 by wt.). **a** Laser emission spectrum with various pump energies. **b** Laser peak intensity as a function of pump energy. Intersection of two lines shows threshold for laser emission. *Red arrow* shows threshold. **c** The plots of pump energy and output energy. Slope efficiency is determined. *Red arrows* show threshold

Similar results for two types of slope efficiency were reported in organic DFB polymer laser based on poly[(9,9-(dihexyl)-9H-fluorene-2,7-vinylene)-co-(1-methoxy-4-(2-ethylhexyloxy)-2,5-phenylene-vinylene)] (poly(DH-PFV-co-MEHPPV)) [13]. As discussed in previous report [13], the reduction of the slope efficiency at higher pump energy is due to the nature of lasing performance of the material of interest, not to degradation by high pump energy, nor to saturation effect [13]. High slope efficiency at lower pump energy region is mainly due to ASE.

In the former study [14], laser emission characteristics and performances were investigated for one- (1D) and two-dimensional (2D) DFB laser devices: high slope efficiency of 7.8% and extremely low threshold of 0.8 nJ were observed for the 2D DFB laser device, whereas low slope efficiency of 2.2% and high threshold of 16 nJ were observed for the 1D DFB laser device. The influence of substrate on 1D and 2D DFB laser emission performance was investigated [15]: slope efficiency of 1.2% for 2D DFB laser device with quartz substrate and 0.65% for that with indium tin oxide (ITO) substrate were observed. Both laser devices had threshold of 35 nJ. Slope efficiency for 1D DFB laser devices with quartz substrate was 0.65% and that with ITO substrate 0.2%.

The laser performances are summarized in Table 2 when Alq_3 host concentration is varied from 20 to 60 wt%. DCM concentration is fixed 1 wt%. It is noted that the lasing peak follows the larger ASE for PS/Alq_3/DCM (69/30/1) as shown in Fig. 1a, whereas the contribution of ASE is smaller for PS/Alq_3/DCM (49/50/1) as shown in Fig. 2a. Lasing threshold is 0.15 mJ cm^{-2} for PS/Alq_3/DCM (49/50/1) is lower than that of 0.23 mJ cm^{-2} for PS/Alq_3/DCM (69/30/1). These results lead to the appropriate concentration of Alq_3 for lasing which is 50 wt%.

Fluorescence spectra are shown for various concentrations of Alq_3 with the DCM concentration fixed 1 wt% in Fig. 3a and those for various concentrations of DCM with the Alq_3 concentration fixed 30 and 50 wt% in Fig. 3b, c, respectively. The fluorescence spectrum with peak wavelength at 500 nm for PS/Alq_3 is appeared at higher energy region, which is also shown in Fig. 3a. That spectrum at higher energy region is due to the fluorescence from Alq_3* in the PS matrix. In all cases, the sample films were excited at 355 nm. All emission spectra in the presence of DCM are that from the fluorescence from the excited DCM (DCM*). In the present case, the large wavelength overlaps between the emission from the excited Alq_3 (Alq_3*) and the absorption of DCM leads to the Förster-type energy transfer to produce DCM*. The efficiency of the fluorescence resonance energy transfer η_{ET} between Alq_3* and DCM is defined as.

$$\eta_{ET} = \frac{1}{1 + \left(\frac{R}{R_0}\right)^6}, \tag{2}$$

where R is the average distance between Alq_3* and DCM, and R_0 is the Förster radius where η_{ET} is 0.5 (50%). Förster radius of 3.25 nm for Alq_3 was already reported [16].

As shown in Fig. 3, in the presence of DCM, only the fluorescence emission from DCM* is observed and no emission from Alq_3*. It means that all excited energy was transferred from Alq_3* to DCM dye through Förster energy transfer process in the fluorescence measurement with low pump energy. Ramos-Oritz et al. investigated the Förster energy transfer from 4,4′-*N*,*N*′-dicarbazole-biphenyl (CBP) to $Ir(ppy)_3$ in polystyrene matrix, and discussed the dynamical change of intermolecular distance between excited CBP (CBP*) and $Ir(ppy)_3$ in the ground state [17]. The increase of pump energy shortens the intermolecular distance between CBP* and $Ir(ppy)_3$ until the former density [CBP*] exceeds the latter density [$Ir(ppy)_3$]. They also studied η_{ET} between CBP* and $Ir(ppy)_3$ as a function of pump energy density, and showed that η_{ET} is constant at pump energy lower than 0.2 mJ cm^{-2}, but it is depressed above that pump energy. It means that some of the excited states produced in CBP will relax without transferring their energy to $Ir(ppy)_3$ when [CBP*] > [$Ir(ppy)_3$], but every excited states produced in CBP encountered $Ir(ppy)_3$ in the ground state to couple with when [CBP*] ≤ [$Ir(ppy)_3$]. At the same region of pump energy density in the vicinity of 0.25–0.3 mJ cm^{-2}, the present slope efficiency for lasing is drastically reduced in the present energy transfer system as shown in Figs. 1c, 2c and Tables 2 and 3. We assume that at the pump energy higher than 0.25–0.3 mJ cm^{-2}, the number density of the excited Alq_3 [Alq_3*] exceeds the number density of DCM in the ground state [DCM], the excess amount of [Alq_3*] will relax without transferring their energy to DCM, and thus this is another reason

Table 2 Summary of laser performances of $\lambda_{L,}$ ASE peak, slope efficiency (SE), and threshold for various concentrations of Alq_3

Alq_3 (wt%)	Angle (°)	λ_L (nm)	ASE peak (nm)	SE (%)		Threshold (SE) (μJ/mJ cm^{-2})		Threshold (peak) (mJ cm^{-2})
20	63.6	–[a]	–[a]	5.4	1.3	0.40/0.17	0.72/0.30	–[a]
30	63.0	621.5	620	6.1	1.8	0.31/0.13	0.60/0.25	0.23
40	63.6	–[a]	–[a]	4.9	1.8	0.35/0.15	0.71/0.30	–[a]
50	60.5	628.0	630	5.8	2.1	0.30/0.14	0.52/0.24	0.15
60	59.5	632.4	635	5.8	1.8	0.28/0.13	0.52/0.25	0.12

DCM concentration is fixed 1 wt%

[a]Not measured

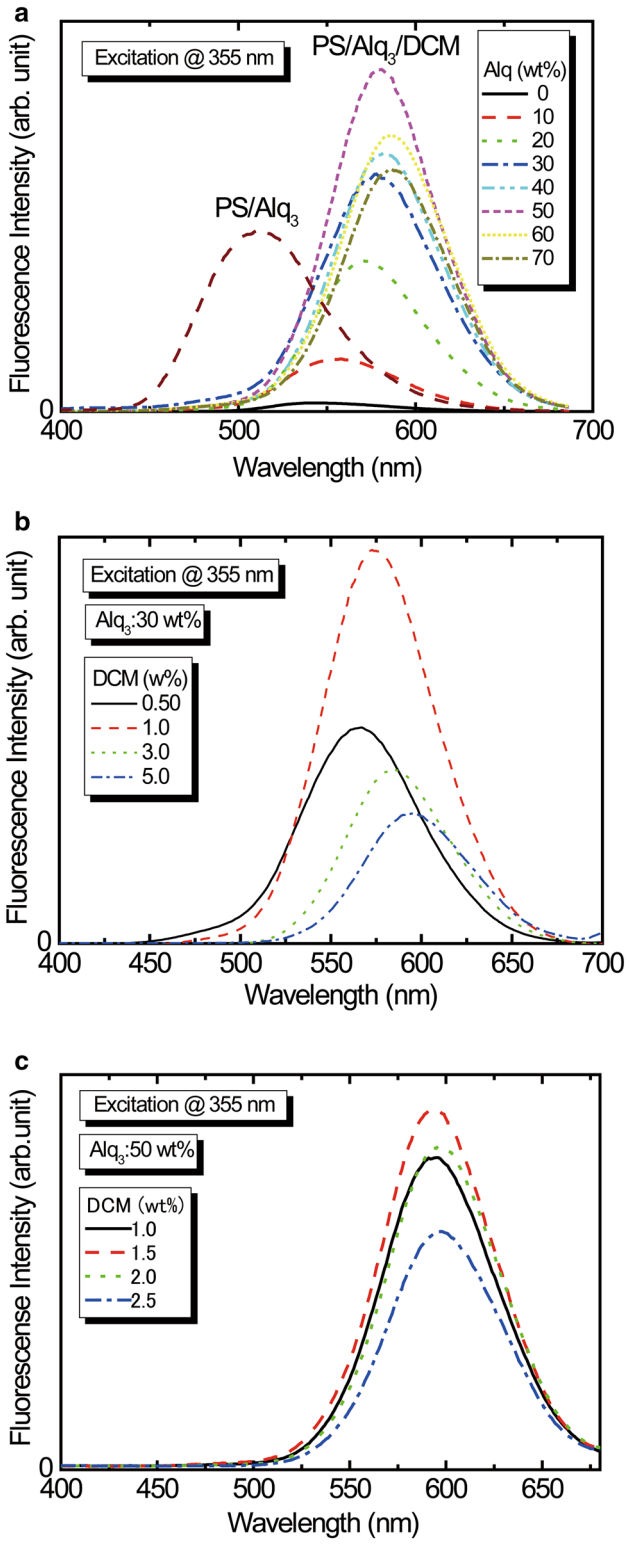

Fig. 3 **a** Fluorescence spectra for various concentrations of Alq_3 in PS/Alq_3/DCM. DCM concentration is fixed 1 wt%. Fluorescence spectrum of Alq_3 in PS/Alq_3 is also shown. **b** Fluorescence spectra for various concentrations of DCM in PS/Alq_3/DCM. Alq_3 concentration is fixed 30 wt%. **c** Fluorescence spectra for various concentrations of DCM in PS/Alq_3/DCM. Alq_3 concentration is fixed 50 wt%

that the slope efficiency is reduced at higher pump energy region.

The DCM concentration dependence of laser performances was investigated by changing the DCM concentration. The obtained results of slope efficiencies and thresholds are summarized for Alq_3 concentration of 30 and 50 wt% in Table 3a, b, respectively. Large depression of the slope efficiency occurs at the DCM concentration above 1 wt% for Alq_3 concentration of 30 wt%, which is consistent with the fluorescence quenching when the DCM concentration is varied as shown in Fig. 3b. For the Alq_3 concentration of 50 wt%, preferred laser performance is revealed at DCM concentration of 1.5 wt%., which is consistent with the fluorescence quenching when the DCM concentration is varied as shown in Fig. 3c.

3.2 Tunable DFB laser performances

As shown in Tables 2 and 3, the peak of ASE was shifted to longer wavelength when Alq_3 and DCM concentrations were increased. It means that the tunable wavelength region for lasing depends on the Alq_3 and DCM concentration. Fluorescence and ASE spectra of PS/Alq_3/DCM film are shown in Fig. 4a, when the sample film was excited at 355 nm. ASE was measured when the sample film was excited by a pulse laser. ASE ranges from 600 to 650 nm. Laser emission for PS/Alq_3/DCM (49/50/1 by wt.) is shown in Fig. 4b. The incidence angle θ ranges from 57.5° to 62.5°, which corresponds to the emission wavelength λ_L ranging from 644.4 to 618.5 nm (tunable region for lasing). The laser emission with the band width less than 0.2 nm was clearly observed. The emission wavelength of DFB laser λ_L is calculated using the equation

$$\lambda_L = \frac{n_{eff}\lambda_p}{m\sin\theta}, \tag{3}$$

where n_{eff} is the effective refractive index, λ_p is the wavelength for pumping excitation, and m is the mode number of diffraction. The emission wavelength λ_L is related to the feedback resonance of microcavity in the DFB structure. n_{eff} was evaluated using Eq. (3) with the incidence angle, the first-order mode $m=1$, and the measured λ_L and λ_p of 355 nm. The evaluated n_{eff} ranged from 1.531 to 1.545, which are shown for each incidence angle in Table 4. For other higher order number mode $m=2$ or 3, the radiation loss (radiation mode) from the waveguide frequently depresses the feedback resonance for lasing. Thus, the laser emission from the first-order mode $m=1$ was employed. Slope efficiency and threshold are plotted as a function of emission wavelength (λ_L) in Fig. 5. Maximum slope efficiency is measured at the emission wavelength in the vicinity between 635 and 640 nm, which is close to the center wavelength of ASE. Maximum

Table 3 Summary of laser performances for various concentrations of DCM

(a) Slope efficiency and threshold at Alq_3 concentration of 30 wt%

DCM (wt%)	SE (%)		Threshold (SE) (μJ/mJ cm^{-2})		Threshold (peak) (mJ cm^{-2})
0.5	4.5	1.3	0.36/0.15	0.62/0.25	–[a]
1.0	6.1	1.8	0.31/0.13	0.60/0.25	0.23
3.0	3.6	0.84	0.33/0.14	0.72/0.30	0.31
5.0	1.8	0.45	0.30/0.13	0.61/0.27	0.35

(b) Slope efficiency and threshold at Alq_3 concentration of 50 wt%

DCM (wt%)	Angle (°)	λ_L (nm)	SE (%)		Threshold (SE) (μJ/mJ cm^{-2})		Threshold (peak) (mJ cm^{-2})
1.0	59.5	624	9.4	2.7	0.20/0.09	0.48/0.23	–[a]
1.5	61.4	631	9.8	3.0	0.18/0.08	0.34/0.17	0.17–0.21
2.0	62.7	633	10.8	2.2	0.27/0.12	0.33/0.14	–[a]
2.5	63.5	635	10.0	2.2	–	0.30/0.13	–[a]

[a]Not measured

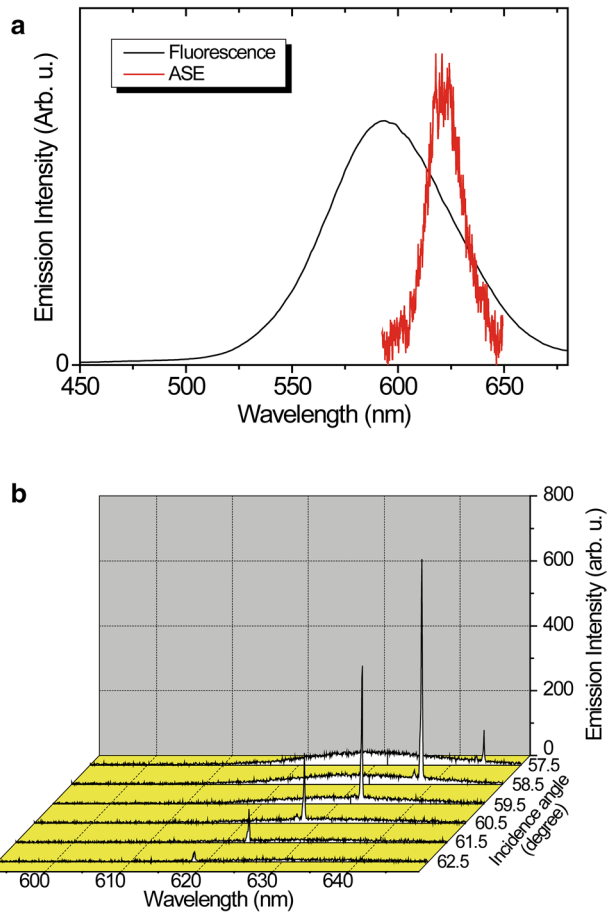

Fig. 4 **a** Fluorescence spectrum and ASE spectrum, **b** laser emission spectrum with various incidence angles between 57.7° and 62.5°

threshold is also measured at 633 nm. Both thresholds are in good agreement within an experimental error.

The effective indices of refraction (n_{eff}*) for TE mode are calculated in a three-layer (air/active layer/glass substrate) waveguide using an eigen value Eq. (4).

$$k_x T = m\pi + \tan^{-1}\left(\frac{\gamma_c}{k_x}\right) + \tan^{-1}\left(\frac{\gamma_s}{k_x}\right) \quad (4)$$

where T is the thickness of waveguide, $k_x = k_0\sqrt{n_f^2 - n_{eff}^2}$, $\gamma_c = k_0\sqrt{n_{eff}^2 - n_c^2}$, $\gamma_s = k_0\sqrt{n_{eff}^2 - n_s^2}$, and $k_0 = \frac{2\pi}{\lambda}$, n_f is the refractive index of the waveguide film, n_c is the refractive index in air, n_s is the refractive index of glass substrate, and λ is the wavelength of the propagated light. Using Eq. (4) with n_f, n_c, n_s, and the observed n_{eff}, we can determine the thickness of waveguide. For PS/Alq_3/DCM (49/50/1 by wt.) waveguide film, T = 227–247 nm was evaluated with n_c = 1.000, n_s = 1.515, n_f of each wavelength determined by the Sellmeier dispersion formula (1), and the observed n_{eff}. Alternative method for the evaluation of the waveguide thickness is the absorbance measurement. For PS/Alq_3/DCM (49/50/1 by wt.) waveguide film, the thickness of waveguide 301 nm was evaluated by the Lambert–Beer law with the absorbance 0.30 measured at 400 nm, the molecular extinction coefficient of Alq_3 7500 l mol^{-1} cm^{-1} at 400 nm reported in the paper [18], and molar concentration of Alq_3 1.31 mol l^{-1} using PS density = 1.2 g cm^{-3}, molecular weight of Alq_3 = 459.2 g mol^{-1}, and the weight percentage of Alq_3. Both thickness measurements are almost in the same order.

Table 4 Summary of tunable laser performances; λ_L, n_{eff}, n_f, slope efficiency, and threshold

Angle (°)	λ_L (nm)	n_{eff}	n_f	Slope efficiency (%)		Threshold (SE) (μJ/mJ cm^{-2})		Threshold (peak) (mJ cm^{-2})
57.5	644.4	1.531	1.657	6.4	2.8	0.25/0.13	0.67/0.34	0.17
58.5	638.6	1.534	1.659	7.4	3.0	0.30/0.15	0.51/0.25	0.17
59.5	633.2	1.537	1.660	7.3	2.8	0.34/0.16	0.51/0.24	0.15
60.5	628.0	1.540	1.661	5.8	2.1	0.30/0.14	0.52/0.24	0.15
61.5	623.2	1.543	1.662	5.7	1.6	0.23/0.10	0.51/0.23	0.14
62.5	618.5	1.545	1.663	–	–	–	–	–

ASE peak @ 630 nm for PS/Alq_3/DCM (49/50/1 by wt.)

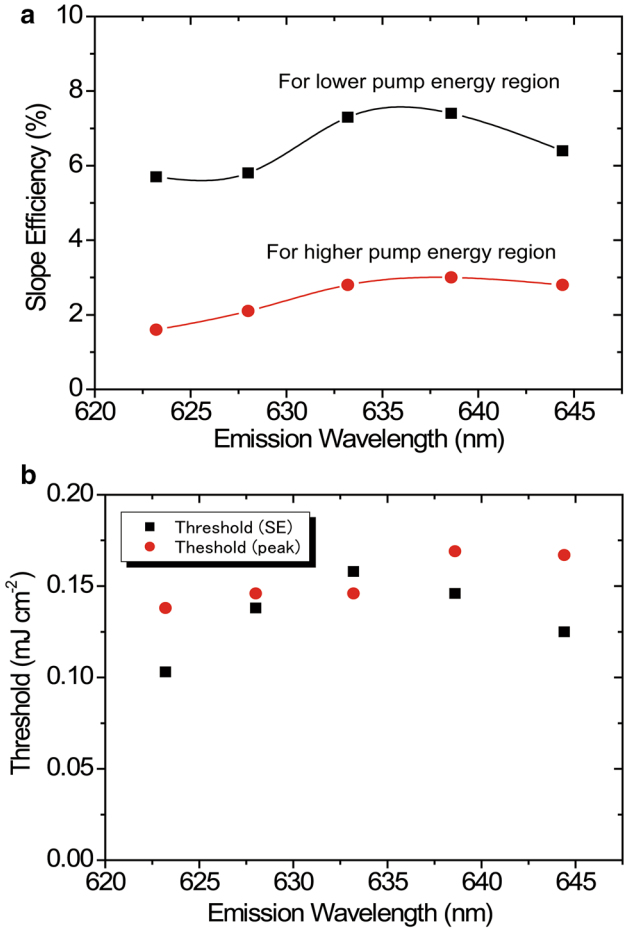

Fig. 5 **a** Plots of slope efficiency as a function of emission wavelength. **b** Plots of threshold as a function of emission wavelength. *Solid curve* in **a** is a guide to the eye

For PS/Alq_3/DCM (69/30/1 by wt.) waveguide film, n_{eff}* was calculated using Eq. (4) with the measured n_f and the thickness of waveguide evaluated. The thickness of the waveguide device 444 nm was evaluated by the Lambert–Beer law with the molecular extinction coefficient of Alq_3 7500 l mol^{-1} cm^{-1} reported in the paper [18], the molar concentration of Alq_3 0.78 mol l^{-1}, and the absorbance of the waveguide film 0.26 measured for PS/Alq_3/DCM (69/30/1 by wt.) waveguide device. The effective index of refraction n_{eff}* = 1.5596 was evaluated using Eq. (4) with the thickness of waveguide of 444 nm, the emission wavelength λ_L = 621.5 nm, n_f = 1.618 determined at λ_L by an one-oscillator Sellmeier dispersion formula Eq. (1). The value of n_{eff}* = 1.5596 is comparable to the effective index of refraction n_{eff} = 1.5601 calculated using Eq. (3).

4 Conclusions

We investigated the DFB laser performances for PS/Alq_3/DCM systems. Alq_3 concentration is varied from 20 to 60 wt% and DCM concentration from 0.5 to 5 wt%. Efficient energy migration among Alq_3 and favorable energy transfer to DCM occur at the composition of PS/Alq_3/DCM (49/50/1 by wt.), which leads to the favorable laser performances. Slope efficiency for ASE and lasing ranges from 4.9 to 10% at the pump energy region lower than 0.25–0.30 mJ cm^{-2}, whereas in the pump energy region higher than that energy density, the slope efficiency in the range of 2.0 and 3.0% is measured mainly due to lasing. The main difference between two slope efficiencies is due to the difference of the ASE contribution. At the pump energy higher than 0.25–0.30 mJ cm^{-2}, the excess amount of the excited Alq_3 molecules is deactivated without transferring their energy to DCM, which leads to the energy loss for lasing. This is another reason for the reduction of slope efficiency at higher pump energy region.

References

1. D.W. Samuel, G.A. Turnbull, Organic semiconductor lasers. Chem. Rev **107**, 1272–1295 (2007)
2. S. Chénais, S. Forget, Recent advances in solid-state organic lasers. Polym. Int. **61**, 390–406 (2012)
3. G. Jordan, M. Flämmich, M. Rüther, T. Kobayashi, W.J. Blau, Y. Suzuki Y, T. Kaino, Light amplification at 501 nm and large

nanosecond optical gain in organic dye-doped polymeric waveguides. Appl. Phys. Lett. **88**, 161114 (2006)
4. J.C. Ribierre, G. Tsiminis, S. Richardson, G.A. Turnbull, J.D.W. Samuel, H.S. Barcena, P.L. Burn, Amplified spontaneous emission and lasing properties of bisfluorene-cored dendrimers. Appl. Phys. Lett. **91**, 081108 (2007)
5. B. Guzelturk, A.L. Kanibolotsky, C. Orofino-Pena, N. Laurand, M.D. Dawson, P.J. Skabara, H.V. Demir, Ultralow-threshold upconverted lasing in oligofluorenes with tailored strong nonlinear absorption. J. Mater. Chem. C **3**, 12018–12025 (2015)
6. M. Berggren, A. Dodabalapur, R.E. Slusher, Stimulated emission and lasing in dye-doped organic thin films with Förster transfer. Appl. Phys. Lett. **71**, 2230 (1997)
7. V.G. Kozlov, V. Bulović, P.E. Burrows, S.R. Forrest, Laser action in organic semiconductor waveguide and double-heterostructure devices. Nature **389**, 362–364 (1997)
8. S. Riechel, U. Lemmer, J. Feldmann, T. Benstem, W. Kowalsky, U. Scherf, A. Gombert, V. Witter, Laser modes in organic solid-state distributed feedback lasers, Appl. Phys. B 71, 897–900 (2000)
9. P.B. Deotare, T.S. Mahony, V. Bulović, Ultracompact low-threshold organic laser. ACS Nano **8**(11), 11080–11085 (2014)
10. N. Tsutsumi, A. Fujiwara, D. Hayashi, Tunable distributed feedback lasing with a threshold in the nanojoule range in an organic guest–host polymeric waveguide. Appl. Opt. 45(22), 5748–5751 (2006)
11. N. Tsutsumi, M. Takeuchi, Ti-sapphire femtosecond pulse pumped laser emission from all-plastic organic waveguide with distributed feedback resonator. Opt. Commun **281**, 2179–2183 (2008)
12. N. Tsutsumi, M. Takeuchi, W. Sakai, All-plastic organic dye laser with distributed feedback resonator structure. Thin Solid Films **516**, 2783–2787 (2008)
13. N. Tsutsumi, H. Nishida, Tunable distributed feedback lasing with low threshold and high slope efficiency from electroluminescent conjugated polymer waveguide. Opt. Commun **284**, 3365–3368 (2011)
14. G. Heliotis, R. Xia, G.A. Turnbull, P. Andrew, W.L. Barnes, I.D.W. Samuel, D.D.C. Bradley, Emission characteristics and performance comparison of polyfluorene lasers with one- and two-dimensional distributed feedback. Adv. Funct. Mater. **14**(1), 91–97 (2004)
15. E.B. Namdas, M. Tong, P. Ledochowitsch, S.R. Mednick, J.D. Yuen, D. Moses, A.J. Heeger, Low thresholds in polymer lasers on conductive substrates by distributed feedback nanoimprinting: progress toward electrically pumped plastic lasers. Adv. Mater **21**, 799–802 (2009)
16. V.G. Kozlov, V. Bilovic, P.E. Burrows, M. Baldo, V.B. Khalfin, G. Parthasarathy, S.R. Forrest, Y. You, M.E. Thompson, Study of lasing action based on Forster energy transfer in optically pumped organic semiconductor thin films. J. Appl. Phys **84**, 4096–4108 (1998)
17. G. Ramos-Oritz, Y. Oki, B. Domercq, B. Kippelen, Förster energy transfer from a fluorescent dye to a phosphorescent dopant: a concentration and intensity study. Phys. Chem. Chem. Phys. **4**, 4109–4114 (2002)
18. M.M. El-Nahass, A.M. Farid, A.A. Atta, Structural and optical properties of Tris(8-hydroxyquinoline) aluminum (III) (Alq_3) thermal evaporated thin films. J. Alloys Compounds **507**, 112–119 (2010)